Fibers and Polymers 2006, Vol.7, No.2, 146-157

Vorticity Analysis Associated with Drafting Cylinders for Pneumatic Spinning

J. M. Bergada*, E. Valencia[1], and Ll Coll[1]

Fluid Mechanics Department, ETSEIAT, Colon 11 E-08222 Terrassa, Spain
[1]Research Textile Institute, INTEXTER, Colon 15 E-08222 Terrassa, Spain
(Received October 24, 2005; Revised May 30, 2006; Accepted June 8, 2006)

Abstract: Traditional spinning systems have reached profitability limits in developed countries due to high production costs and low system productivity. Pneumatic spinning is seen as a developing system, because productivity is much higher than conventional systems. This study evaluates one of the main problems to increase productivity in pneumatic spinning, where air mass-flow is dragged by the drafting cylinders. This flow interacts with the incoming fibres deviating them from their expected path. Via laser anemometry, airflow velocity distribution around drafting cylinders has been measured and it has been found that vorticity is created at the cylinder's inlet. Extensive CFD simulation on the air flow dragged by the cylinders has given a clear insight into the vortex created, producing valuable information on how cylinder design affects the vorticity created. Several drafting cylinder designs have been tested without giving any improvement in productivity. However, the use of a drafting cylinder with holes in it produced good results to the problem of air currents, strongly reducing them and therefore allowing a sharp increase in yarn quality, as well as an increase in productivity. An extensive study on vortex kinematics has been undertaken, bringing with it a better understanding of vortex creation, development and breakdown.

Keywords: Drafting cylinders, Pneumatic spinning, Laser anemometry, CFD simulation, Vortex kinematics

Introduction

The textile industry in the European Union is adapting to low production quantities, due to current ever-changing fashion trends. Therefore, textile processes and materials must frequently be changed. Flexibility in the textile industry seems to be the key to success. Quality and reliability must be maintained to achieve the highest quality standards while at the same time maintaining or reducing production costs. However, the textile industry must also be environmentally aware.

This current trend affects the entire textile industry and in particular, spinning processes because they require high investment due to the complexity and dimensions of the facilities.

Not all of the requirements listed above can be accomplished with current technology. It is therefore necessary to develop a more advanced yarn production technology because the conventional system shown in Figure 1(a), which is currently responsible for 98 % of the world's yarn production for a yarn count below 20 tex, is no longer able to reach the productivity standards required. The main problem with conventional systems is a production rate limit of 15-25 m/min.

Other systems, such as OE-rotor in Figure 1(c) have a much higher productivity rate although due to the main features of the process, it is not economically viable to produce yarn for a count below 20 tex. Nevertheless, it is estimated that around 1.7 % of global yarn production for a yarn count below 20 tex is produced by the OE-rotor system [1].

European textile enterprises will see a huge increase in production costs as a consequence of the increasing cost of conventional machinery acquiring, the cost of intelligent systems implementation on machinery, logistical production systems and systems to improve and ensure product quality etc.

The conventional spinning system has several inherent disadvantages when processing; low productivity derived from high centrifugal forces and existing frictions between the yarn and the traveler. To overcome these disadvantages, it has been necessary to reduce spindle size by 50 %. This has allowed spindle speed to increase to 20000 rpm. However the need to use smaller dimension spindles makes connecting the winding to the spinning machine essential, and therefore considerably limits process flexibility, especially when dealing with lower production quantities. For example, it can be said that a spinning plant with 8 ring-spinning machines of 1000 spindles each, needs an average cleaning time of 6 hours per batch change per machine.

This is the reason why profitability is only achievable when larger quantities of production are involved, production runs which last at least 4 weeks, involving more than 100 Tm of raw material, figures relatively far from present market trends.

According to the aforementioned, the conventional process has reached its technological limit, with its life expectancy being cut short in developed countries due to low competitiveness and with the related loss of economic potential, (losing 975 million Euros annually which corresponds to 2000 SME'S), causing job losses (in the machinery construction sector) and 1400 million Euros in losses for the spinning factories.

Around 1980, the Japanese company Murata Machinery Ltd. introduced a new spinning system called pneumatic

*Corresponding author: bergada@mf.upc.edu

wrapping spinning, with false wrapping twist through a tandem nozzle. The system consisted of creating a fluid vortex that gave some torsion to part of the incoming fibres, wrapping them around a fibre nucleus and forming a yarn, the torque being produced via a tandem nozzle Figure 1(b). This is a valid system for producing yarn of a mixture of cotton and chemical fibres at high speed between 150 and 300 m/min [2-5]. Despite advantages such as high productivity, this spinning system has not yet been fully accepted within the European market, mainly due to the peculiar structural properties of the yarn produced, which limits its use with certain fabrics.

The most recent advances in air jet spinning are claimed to have been made by the Murata Company, which at the last Birmingham (UK) ITMA 2003 exhibition, presented the new Muratec (J) "vortex" MVS 861 model-spinning machine [6]. The maximum production speed of this machine is 450 m/min, it also achieves yarn quality and energy efficiency which are mainly due to the use of a new set of nozzles, which operate under real wrapping twist [7].

General View of Spinning Units and Their Main Developments

The different existing spinning units are shown in Tables 1, 2 and Figures 1, 2. Figures 1 and 2 give schemes for the different spinning units and twisters. Table 2 indicates some of the latest research on spinning units and the main development found. It describes the combination drafting/twister used in every study and yarn features in each case. Table 1 describes the basic operative systems used in the research as defined in Table 2. In the first part of Table 1, the main existing drafting systems are evaluated as well as their main features. In the second part, the methods used to create twist are analyzed according to the yarn structure, production speed and yarn title.

From the information gathered, it can be concluded that pneumatic spinning is the fastest method to produce yarn and despite the limitations on the set of titles able to be produced, it seems it has great potential for the near future. However, it does appear as if thorough research on pneumatic spinning has not yet been carried out. This paper will therefore focus on analyzing the main problems, which could prevent further production increase.

Recent developments on pneumatic nozzles obtained at INTEXTER-UPC, thanks to BRITE-EURAM-CT-96-0324 CICYT (TAP97-1444-CE) project, have shown that velocities of 600 m/min can be achieved [18]. Thanks to this study, it was noticed that production speed is limited by two factors; the real wrapping twist nozzle and the drafting system. It was also observed it is necessary to solve several fluid mechanics problems that appear in the drafting system to increase speed. The main problem is the apparition of airflows at the inlet of the drafting rollers. This air mass-flow generated by the cylinders, act on the incoming yarn fibre-flow causing a misalignment of some of the fibres, and displacing them from original fibre flow direction to the axial one, Figure 3. Thorough research is being undertaken at INTEXTER-UPC in order to overcome such a drawback.

Table 1. Main drafting systems and methods to create twist

Drafting Function:	Different kinds	Permeable cylinders with suction	SIROS	Geometry modifiable	Loading cylinders system	Conventional standard	Disgregator
Fiber flow constriction	Fiber flow	Continuum	Continuum	Continuum	Continuum	Continuum	Not continuum
Fiber adaptation to be twisted	Fiber adaptation to be twisted	A; D	A	A; B; D	A; B; D.	A; B; D;	C; D;

Twist Function	Different kinds	Ring spinning	Pneumatic spinning			OE-Rotor	OE-friction spinning	Repco
	Method to create twist	Mechanic	Fluid mechanic			Mechanic	Mechanic	Mechanic
Fiber flow stabilization, Transfer physical properties to the yarn (Mechanical resistance, flexion, etc.)	Yarn structure	Helicoidally uniform	Fibers of the nuclei	MJS parallels	MVS parallels	Presents torsion	Random	Similar to a yarn with two ends.
			Wrapping	(a)	(b)	Random direction		Conventional, with alternating twist direction.
(a) Random direction of the twist. S o Z	Production velocity (V m/min)	< 30	< 400			< 300	< 300	200
(b) Single direction of the twist	Set of titles	No limits	8 ÷ 60 tex			20 ÷ 100	140 ÷ 3000	50 ÷ 2000

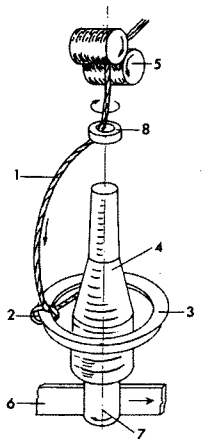

1. Yarn, 2. Traveler, 3. Ring, 4. Spindle, 5. Drafting roller, 6. Belt drive, 7. Pulley, 8. Thread guide

(a) Ring spinning

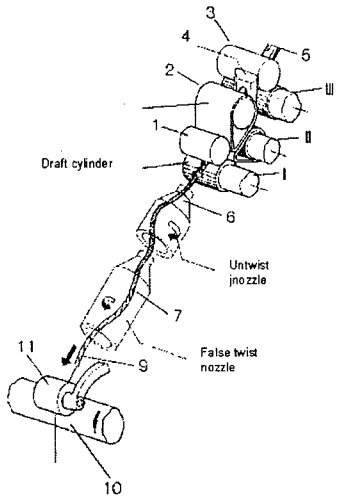

1/I. Drafting rollers, 2/II. Aprons, 3/III. Feed cylinders, 4. Condenser, 5. Sliver, 6. Untwist nozzle, 7. False twist nozzle, 9. Yarn, 10, 11 Production cylinders

(b) Pneumatic spinning

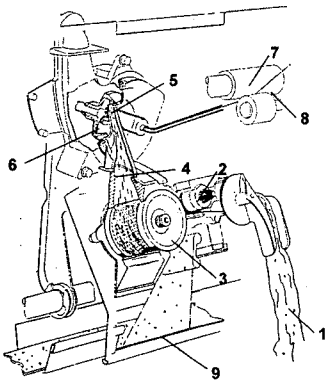

1. Fibre sliver, 2. Condenser, 3. Disgregator, 4. Guiding fibres nozzle, 5. Output element, 6. Rotor, 7. Extracting cylinders, 8. Yarn, 9. Impurities

(c) OE – Rotor spinning

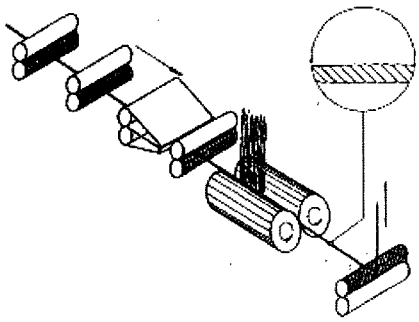

(d) OE – Friction spinning

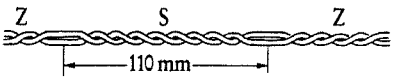

Repco yarn

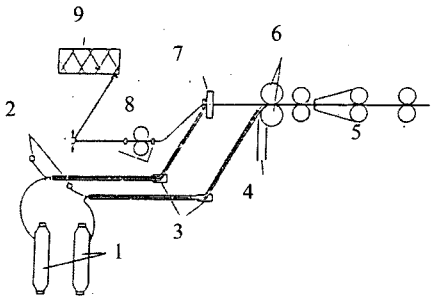

1. Feeding yarn, 2. Transducers, 3. Air injection, 4. Suction, 5. Drafting system, 6. Rubbing cylinders, 7. Friction discs, 8. Tension pulley, 9. Bobbin

(e) Repco

Figure 1. Different systems to create twist.

This paper focuses on the understanding of air mass movements and their evolution at the inlet of the drafting rollers. It is important to note that there is a precedent for the flow around two rotating cylinders. This flow was studied by Ludwig Prandtl [19] in which he considered the instability of the shear layer created.

Experimental and Simulation Results

Laser Anemometry Measurements

Test Rig to Measure Velocity Distribution

In order to find the air velocity distribution around the

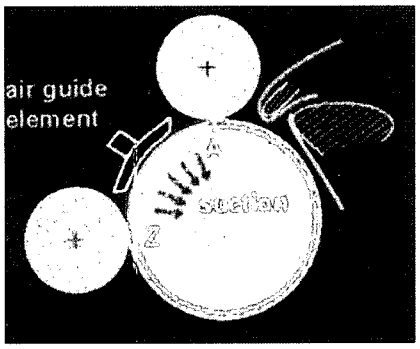

(I) Permeable cylinders with suction

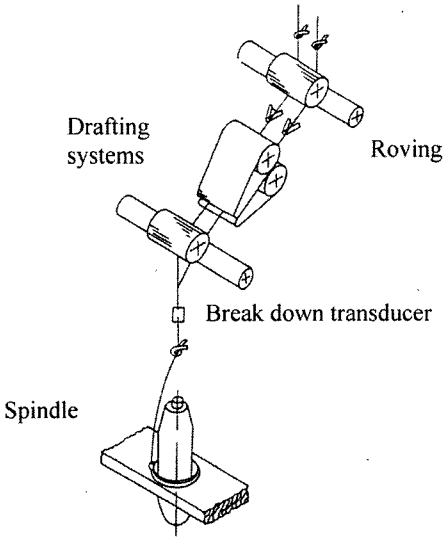

(II) SIROS

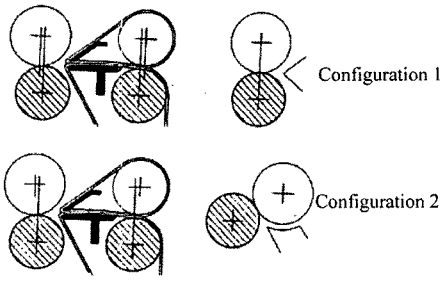

(III) Geometry changeable

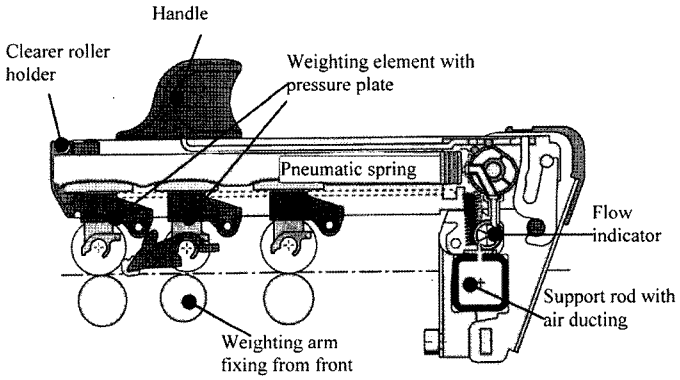

(IV) Loading cylinders system

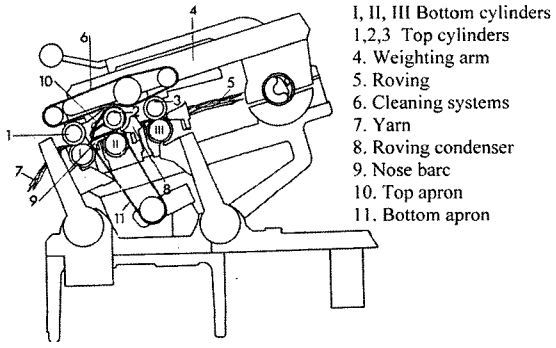

(V) Conventional standard

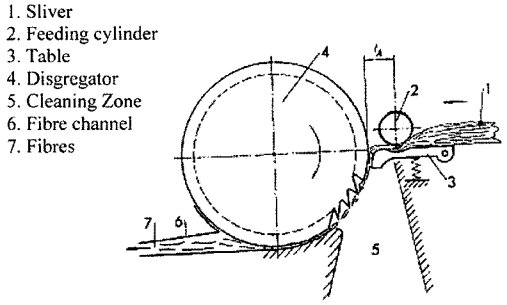

(VI) Disgregator

Figure 2. Several drafting systems.

Table 2. Latest research on spinning units and the main development found

References	Coll *et al.* [8]	Stalder *et al.* [9]	Ben Hassen *et al.* [10]	Duru *et al.* [11]	Lünenschloss *et al.* [12,13]	Artzt *et al.* [14]	Cheng *et al.* [15]	Taylor *et al.* [16]	Artzt [17]	INTEXTER Research		
Main development	Analytical study of the creation of alternative torsion.	Produces a general revision, (state of the art).	Use of condensers Modifies distance between cylinders.	Modify velocity	Study on the torsion and fibre flow in the yarning chamber.	Optimise the process via modifying the geometry.	Compares yarn properties.	Study the influence of the upper cylinder hardness.	Envelope amplified -cylinder speed.	Aerodynamic behaviour of different high speed drafting systems. Development of different drafting systems for high speed pneumatic spinning		
Consequences	I-E (Repco)	Combination I-A compared with V-B	Compares III-A y IV-A	VI-C (open end)	VI-C (open end)	I-A compared with V-A	I-A compared with V-A	III-A	III-A		V-B	VI-B
	Optimisation of the torsion distribution.	The process V-B is the most expensive and shortest one.	Decreases the process steps. Increases evenness regularity. -CV -Neps	Increases evenness regularity -Neps	Optimization of yarning behaviour	Increases regularity.	Increases regularity. -CV -Neps -Hairiness	Increases regularity -CV	Improves regularity -Sliding aprons	Aerodynamics	Deficient	Acceptable
										Textile regularity	Optimum	Deficient

Table 3. Laser anemometer, main characteristics

Laser type	Maximum power	Wavelength	Focal length	Beams separation at the outlet	Measurement volume length	Separation between lines
Argon	750 mW	514,5 nm	310 mm	38 mm	0.38 μm	2.08 μm

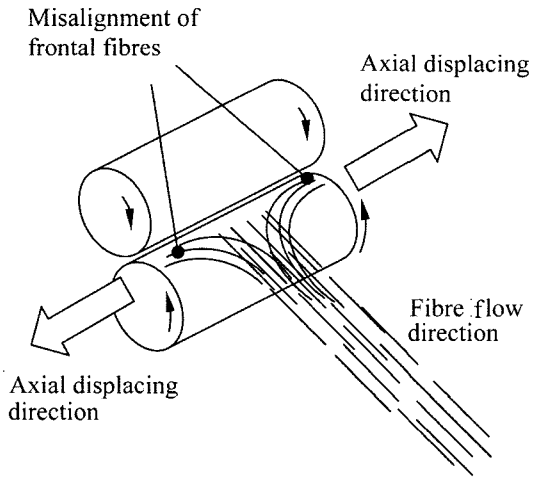

Figure 3. Fibres misalignment at the entrance of the drafting cylinders.

spinning cylinders, a laser Doppler velocimetre was used. Its main features are shown in Table 3.

The fluid used as a contrast was smoke SAFEX Std. the measuring conditions being $P_{absolute} = 101600$ Pa; $T = 289$ K. The different parts of the test rig used in this experiment are detailed in Figure 4(a). On the left is the computer used to record the data. There is a BSA spectral controller just below the computer and the laser anemometer is on the right hand side of the computer. To the right of the picture is the laser head.

The argon laser anemometer produces two beams (as shown in Figure 4b) which intersect at a given point. In fact, this point is a volume measure in which a set of light fringes is created. When a flow particle crosses the fringe volume, the light is reflected and the laser measures the pulsation of the reflected light and then finds the pulsation frequency via a discrete fast Fourier transformation. The particle velocity is proportional to this frequency. The proportionality is given by the equation:

$$V = fC \tag{1}$$

Where, f: frequency (Hz)
V: velocity (m s^{-1})
C: constant (m s^{-1} Hz^{-1})

The constant value for the anemometer used is $C = 3950$ (m s^{-1} MHz^{-1}).

It should be taken into account that the laser anemometer will give a distribution of the measured velocity after taking 3000 measurements at each point, assuming a normal distribution. The anemometer calculates the average velocity of each measure and the variance and the graphs represented will show the average measure at each point.

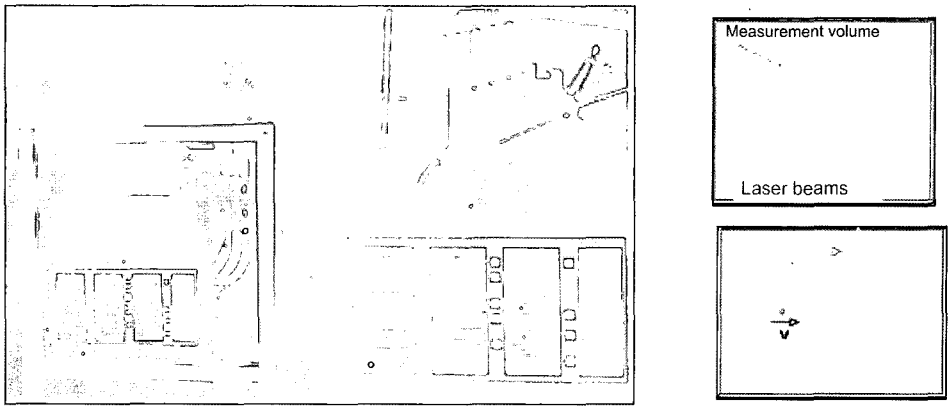

Figure 4. (a) Main parts of the argon laser anemometer, (b) laser working principle.

Velocity Measuring Procedure

Test measurements were focused on finding air velocity distribution around the inlet and outlet of the drafting rollers. Measurements were taken along the cylinder axis at 3.5, 7, 11, 17.1, 23.2, 28.3, 33.5, 37.5, 41 mm and at each axial point a set of radial points were chosen, which were 0.2, 0.6, 1, 1.4, 1.8, 2.2, 2.6, 3, 3.4, 3.8, 4.2 mm. Radial measures were taken against the cylinder surface; as shown in Figures 5 and 11.

Measurements were taken at several angles versus the cylinder contact point, 45, 60 and 90 degrees. Measurements were also taken at the cylinder inlet and outlet and on both upper and lower drafting rollers. The main dimensions of the drafting rollers are defined in Table 4 model 1.

From these measurements, a set of graphs was obtained. The graphs show a clear reduction of dragged velocity with radius as had been expected. In addition, there is great uniformity when comparing the velocity reduction at different axial points. It is interesting to note that at some angles, mainly at 45 degrees, the tangential velocity changes its sign, as shown in Figure 5. This clearly indicates that air masses must turn at some point and this effect could give some explanation to fibre distortion at the drafting roller inlet.

From Figure 5, it can be stated that air seems to be turning at the centre of the cylinder, axial distances of 17.1; 23.2; 28.3 mm, while this rotation of air seems to disappear at cylinder edges. It seems that a vortex is generated at the cylinder centre and this vortex dissipates when it reaches the outer edges.

Numerical Simulation of Air Currents

Although high productivity was achieved via pneumatic spinning due to the work carried out in the BRITE-96 project it can be seen during experiments that some fibres at the stretching cylinders inlet do not follow the theoretical path. As a result, some of them are dragged towards the cylinder sides, being incorrectly trapped by the drafting cylinders.

Measurements during testing have given a first approximation of what happens at the drafting rollers inlet and it appears as if air dragged by the cylinders is the main cause of the problem. It was therefore decided to carry out a 3D-CFD model of the drafting rollers in order to get a better understanding of the air currents involved and their evolution.

Since the model had to simulate the air movement at the

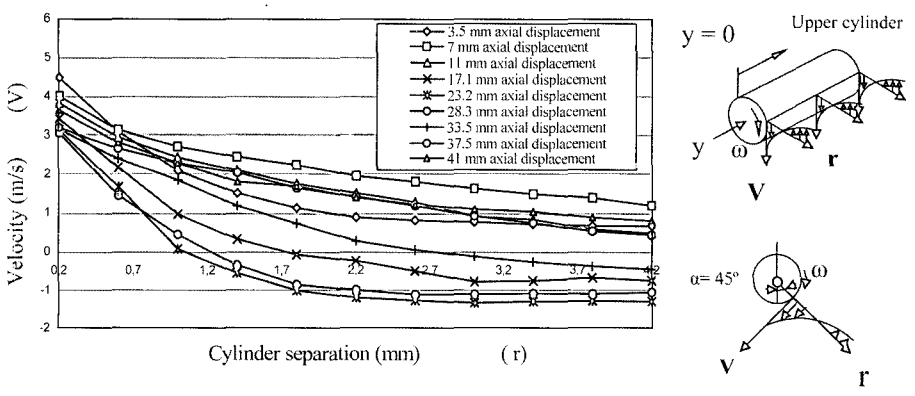

Figure 5. Tangential velocity distribution versus radius for a set of axial positions. Upper cylinder, 45 degrees.

Table 4. Main characteristics of the two CFD models of the drafting rollers

Main characteristics	Model 1	Model 2
Diameter of upper stretching cylinder	55 mm	28 mm
Diameter of lower stretching cylinder	64 mm	64 mm
Gap between cylinders	0.3 mm	0.3 mm
Angular velocity upper cylinder	363.64 rad/s	714.3 rad/s
Angular velocity lower cylinder	312.5 rad/s	312.5 rad/s
Total cylinders length	22.5 mm	22.5 mm
Total cells generated on the grid	3100000	3500000
Surface roughness	5 microns	5 microns

cylinder inlet, it was decided to represent just half of each cylinder and pay special attention to building a very accurate grid near the contact point. Two models were built with different upper cylinder diameters. The main features of the models are described in Table 4.

Due to the large amount of cells created, it was decided that a computer with huge amount of RAM would be used. In this case, a supercomputer Alpha Server GS 1280 32 with 32Gb RAM and 16 processors was used. The computer is located at the Centre for Super Computation in Catalonia, in Barcelona. Each run needed around 30 hours to achieve convergence when using three processors. The software used to perform the calculations was FLUENT version 6.12. The turbulence model employed was k-ε RNG.

General Overview of the Simulation

Figures 6(a) and 6(b) show some results from the 3D-CFD model. Figure 6(a) represents a view of the air mass at the stretching cylinders inlet, where the vorticity created can clearly be seen in front of the cylinders. At this point, a lower and upper vortex appear, which are both rather similar. It appears as if the vortex is pulling fluid from inside the cylinders inlet towards the exterior part. It is also interesting to point out that the vortex centre in the upper cylinder is located at

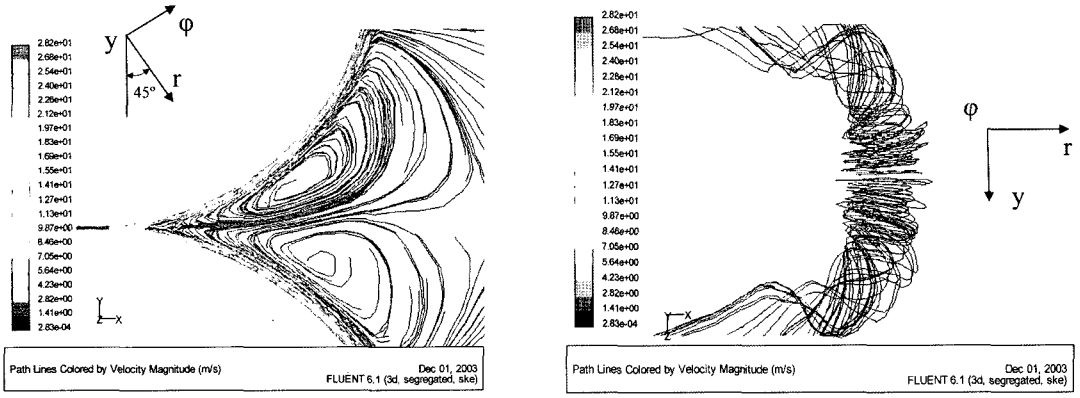

(a) (b)

Figure 6. Vortex created at the entrance according to CFD model 1; (a) normal section to the cylinder axis and (b) axial section, along the cylinder axis, plan view.

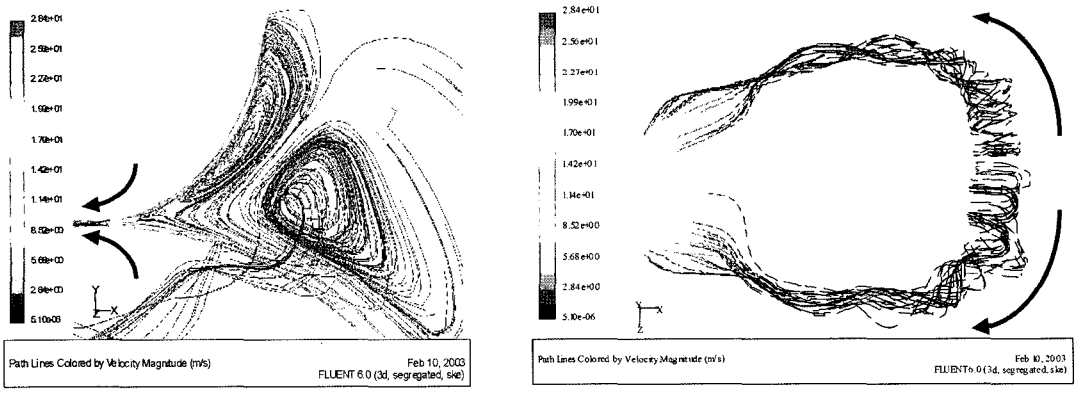

(a) (b)

Figure 7. Vortex created at the entrance according to CFD model 2; (a) normal section to the cylinder axis and (b) axial section, along the cylinder axis, plan view.

45 degrees versus the vertical axis that joints both cylinder centres. This has viable correlation with the experimental results shown in Figure 5. Figure 6(b) is an upper view of the upper vortex, where it can clearly be seen that air forces the fibres to turn, and at the same time pulls them axially towards both ends of the cylinder. This is a good explanation as to why fibres disperse at the stretching cylinders inlet. It can also be seen that vorticity disperses as the fluid reaches the cylinder edges and again this effect matches the experimental results.

Figures 7(a) and 7(b), show the vortex created when the upper cylinder is much smaller than the lower one, (see model 2 in Table 4). It can be seen that the upper vortex is much smaller than the lower one. When looking at the upper vortex from above in Figure 7(b), it can be concluded that as the vortex decreases in size, it maintains its structure longer. Furthermore, when comparing Figures 6(b) and 7(b), it can be seen that the vortex in Figure 7(b) maintains its shape somewhat longer than in Figure 6(b). The vortex intensity is expected to increase as the vortex decreases in size.

It is important to note that in Figure 7(a), the lower vortex is located at the fibre flow path, which therefore means that fibre distortion is expected to be much higher with this cylinder configuration. Experimental tests with the spinning unit confirmed this theory.

Specific View Simulation

At this point, it was clear that vorticity is created at the cylinders inlet, and this vorticity is what prevents an increase in production speed. To solve the problem, it is necessary to dispose of these turning air masses, or maybe just direct them appropriately. At first, it was thought that if one of the cylinders (the lower one) had longitudinal grooves cut into it, it might be enough to allow some air to pass through the gap between the cylinders and therefore decrease the turning air mass at the inlet. This kind of cylinder is shown in Figure 8(a), with some 2D CFD results in Figure 8(b). It is noted that some vorticity is still created inside the grooves, and that large-scale turbulence vortex still appears at the inlet. During testing, it was found that such a cylinder was still creating large fibre disturbances, preventing a further increase in productivity.

The second cylinder analyzed was the OS21-62, shown in Figure 9(a). This particular type of cylinder had the advantage over the previous one in that the grooves were also open in the fibre direction. A reduction of turning mass at the inlet was predicted and took place. However, it was also noted that some fibres were not appropriately pulled towards the pressing point between cylinders due to the discontinuity of

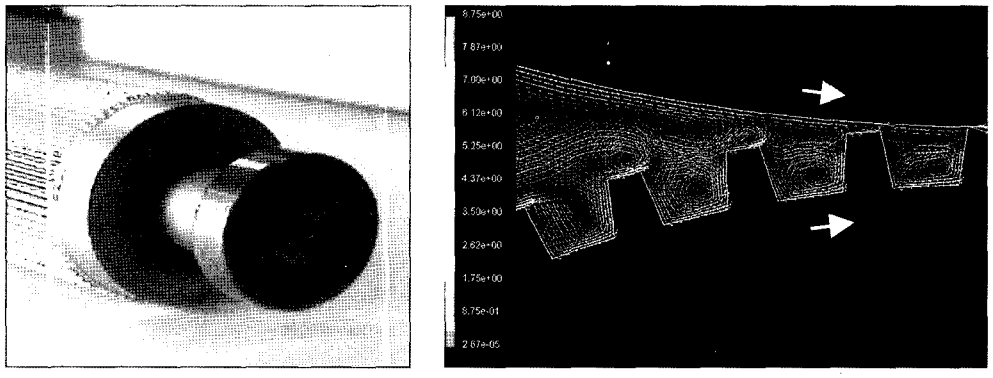

(a) (b)

Figure 8. (a) Lower cylinder with grooves, (b) simulation at 400 m/min.

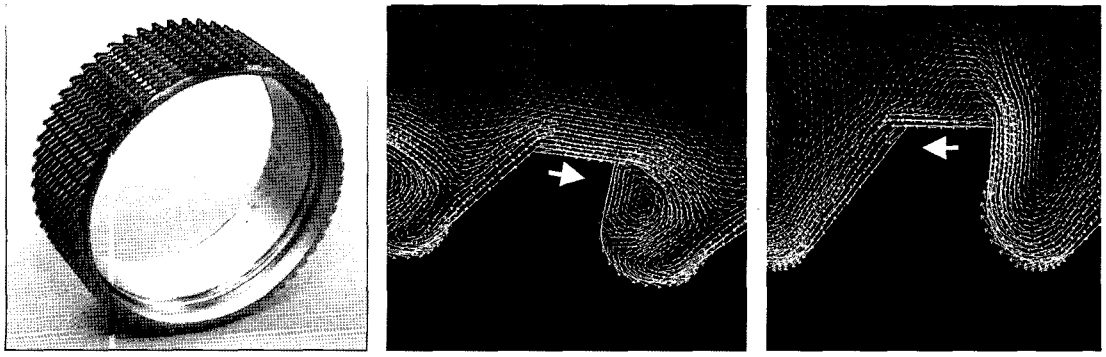

(a) (b) (c)

Figure 9. (a) Lower cylinder Type OS21.62, (b) turning clockwise, and (c) turning anticlockwise.

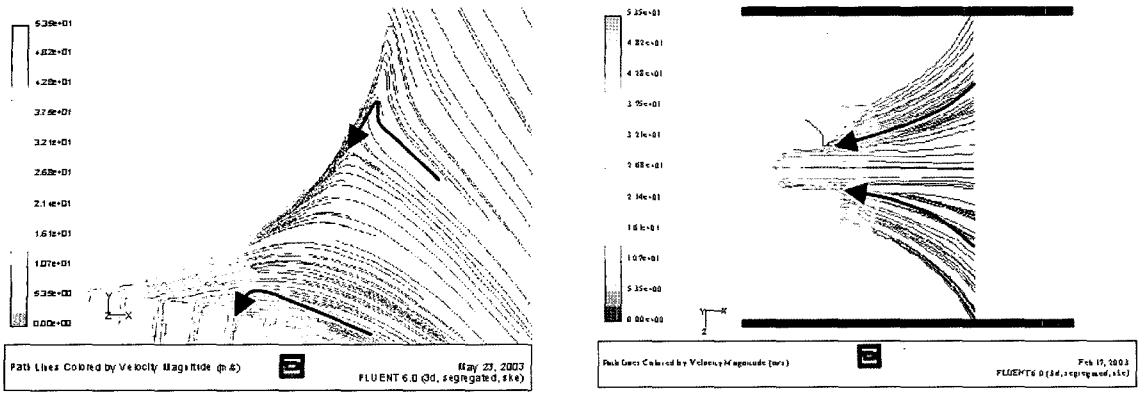

(a) (b)

Figure 10. CFD flow simulation at the cylinders inlet when the lower cylinder is porous; (a) normal section to the cylinder axis and (b) axial section, along the cylinder axis, plan view.

the pressing line. In Figures 9(b) and 9(c), the vortex created around the grooves is shown when the cylinder turns in opposite directions. Figure 9(b) shows a tiny vortex appearing at each tooth. When testing this cylinder it was found that the fibres were being wrapped together forming small balls (neps), at speeds near 500 m/min of tangential velocity, and consequently the quality of the yarn produced sharply decreased.

In order to avoid formation of neps, configuration 9(c) was used. In this case, fibres tended to be expelled out from the cylinders path but were not pulled appropriately due to insufficient pressing points between cylinders. As a result, velocity production could not be improved.

At this point, it became clear that cutting grooves would not give any further increase in machine production, therefore research, at INTEXTER-UPC took a different path. The solution came when studying the flow behaviour for a lower cylinder with tiny holes, as shown in Figure 10. Via creating a suction in the interior of the cylinder, it was possible to direct the air currents created at the cylinders inlet, and then to pull the fibres without any fibre loss or wrapping. Figure 10 shows a simulation of the flow at the cylinders inlet, where it is noticed the perfect flow path.

Some of the main advantages found when using a lower cylinder with holes are, as follows;

- The yarn quality is sharply increased, meaning that the yarn has no NEPS.
- Increasing production speed will only depend on nozzle performance.

It can therefore be established that this solution will enable future spinning machines achieve better performance.

Analysis and Discussion

Determination of the Main Flow Features. Flow Quantification

Once the air pattern is determined mainly via simulation,

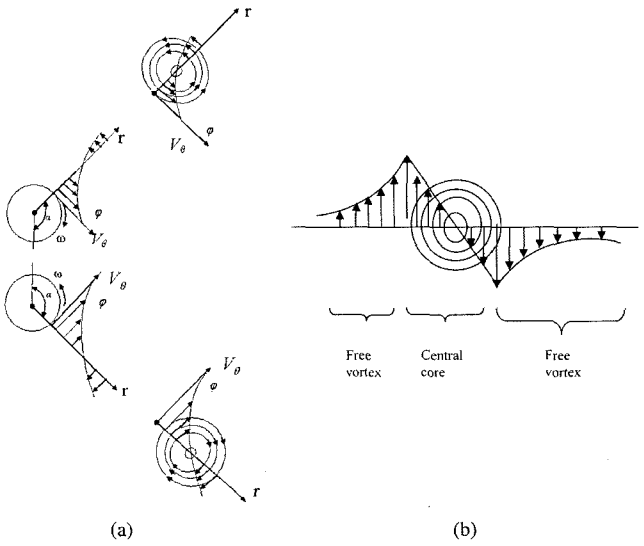

(a) (b)

Figure 11. (a) Main pattern of the measured velocity distribution according to Figure 5, normal section to the cylinder axis. The streamlines of the vortex created have been added due to the cylinder turning (central core), (b) Theoretical velocity distribution of a forced vortex.

and experimentally, the main flow features can be analyzed mathematically.

Phenomenology

When checking the experimental results given in Figure 5, it should be noted that air velocity distribution measured at 45 degrees from the upper cylinder inlet is fairly similar to the typical distribution produced by a forced vortex, which constitutes the nucleus of a potential vortex as shown in Figure 11. Therefore flow is expected to turn as demonstrated via simulation.

The results of the numerical simulation via finite volumes

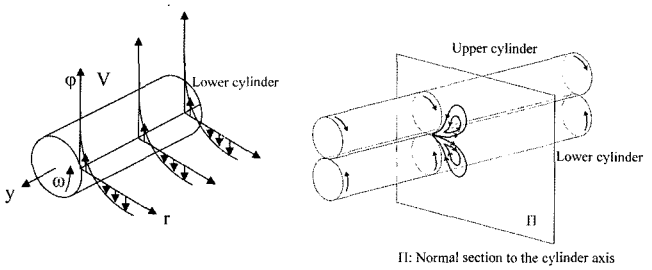

Figure 12. Velocity distribution and vortex associated along the cylinder length.

confirmed the velocity values obtained during testing. From the numerical simulation, it was very clearly seen that streamlines at the cylinders inlet had a similar shape to concentric circumferences, which obey the same flow pattern as found experimentally. This pattern is outlined in Figure 12.

In reality, what appears at the stretching cylinders inlet is a pair of vortexes A, B, as shown in Figure 13, whose streamlines turn in opposite directions. This happens because the turning cylinders that create this air rotation turn in opposite directions as well. As the turning cylinders, which can be regarded as vortex generators have different diameters, the vortex configurations also appear to have different dimensions (see Figures 6 and 7). In general, it can be said that for a constant turning speed, the bigger the cylinder diameter the bigger the tangential velocity and therefore the mass of air being dragged is also greater. As a result, the vortex generated will also have a larger diameter and the associated intensity is expected to decrease as the vortex diameter increases. When maintaining a constant tangential velocity, the smaller the cylinder diameter the smaller the vortex generated and the quicker the vortex turning speed as shown in Figure 7, vortex intensity increases.

When studying the air mass behaviour tri-dimensionally, which is the evolution of several streamlines for different axial distances, as shown in Figure 12, a general streamline appears which indicates that the movement of the fluid particles has an helicoidally shape, and flow moves axially from the cylinder centre towards both ends. It can be seen from Figures 6(b) and 7(b) that the angle the vortex helix forms with the cylinder longitudinal axis is less than 2 degrees, therefore, means that helixes will maintain their shape fairly consistently along the cylinder axis.

This flow behaviour is similar to the flow seen in the seals between impeller & casing and diffuser & casing of an axial turbine where two vortexes can be distinguished. They are known as the channel vortex and the seal vortex and are important when evaluating secondary energy losses [20].

At both ends (C1 and C2) of the rotating cylinders in Figure 13, the vortex tube experiences a sudden change, since the tangential velocity from the cylinders does not exist anymore and the vortex tube can no longer continue. As a result, the streamlines tend to separate producing an increase in vortex tube diameter. The vortex helix also increases causing the dissipation of the flow, which accompanies deceleration of the external stream and vortex breakdown.

It must be pointed out that according to the laser Doppler measurements in Figure 5, it appears that the vortex tube dissipates before reaching the cylinder ends.

Vortex Kinematics

In order to get a quantification of the vorticity created, it was decided that a kinematical study of the flow would be carried out. To do so, cylindrical coordinates system was adopted (y, r, Φ) whose corresponding velocity components are (u, v, w), (see Figure 14). The vorticity components on each axis have been defined as (ω_y ; ω_r; ω_Φ). The relation between the vorticity components and the velocity ones are given in Table 5 which represents a steady axis-symmetric flow with swirl, (component $v \neq 0$), as studied by Batchelor [21].

From velocity values found experimentally using laser-Doppler anemometry, vorticity components were calculated using the equations in Table 5. It is clearly seen from Figure 5 that the dominant vorticity component will be ω_y reducing the vortex line to a line following the "y" direction. In Figure

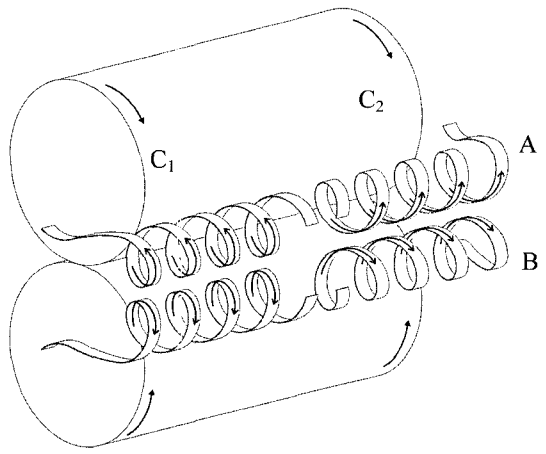

Figure 13. Vortex doublet created at the drafting rollers inlet.

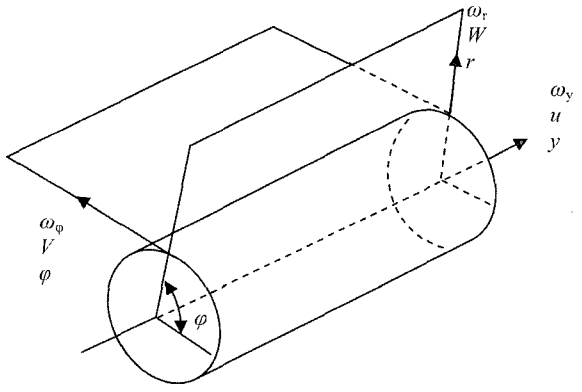

Figure 14. Magnitudes in cylindrical coordinates.

Table 5. Vorticity components in cylindrical coordinates

Name	Velocity components	Vorticity components
Axial	u	$\omega_y = \frac{1}{r}\frac{\partial(rv)}{\partial r}$
Radial	w	$\omega_r = -\frac{\partial v}{\partial y}$
Azimutal	v	$\omega_\varphi = \frac{\partial w}{\partial y} - \frac{\partial u}{\partial r}$

15, the ω_y component is represented at the upper cylinder inlet end and at an angle of 45 °. The result is a surface along the radial and axial coordinates, which can be simplified into two planes, one having a certain pendent (a), and the other horizontal (b). See lower left corner of Figure 15.

To link such results with the flow representation in Figure 6, a stretched vortex filament was used, which can be calculated using equation (2) and taking only into account the horizontal plane (b) in Figure 15 because vorticity is rather constant for that plane. The stretched line ω_y is represented in Figure 16, notice that around vector ω_y the flow streamlines are represented.

A graphical representation of vorticity will allow to understand its influence. This involves obtaining the stretched vortex element as an analogy of the well-known streamlines. Since $\omega_r << \omega_y$ the stretched vortex element will be given by the equation:

$$\frac{\omega_r}{\omega_y} = \frac{dr}{dy} \tag{2}$$

As stated $\omega_r << \omega_y$ therefore $dr/dy \Rightarrow 0$, which gives the equation r = constant. Such a condition represents the stretched vortex filament. In Figure 16, the location of the ω_y vector can be seen, which is parallel to the y-axis, the streamlines induced by ω_y are also represented.

In other words, as the pendent of the vortex line is zero, it will mean that the vortex lines will be parallel to the "y" axis and will be located at a given radius.

Assessment

This consists of determining the power associated to the tube or vortex filament of which intensity is ω_y, and its section is given by the vortex external circular streamline.

For a given position y_1 the circulation associated to the vortex will be determined by:

$$\Gamma_1 = \int \vec{V}_1 \, d\vec{r} = \int rot\vec{V} \, dA = \omega_{y1} A_{vortex}$$
$$= 4 \cdot 276{,}3{,}3 \; 10^{-6} = 0{,}001105 \frac{m^2}{s} \tag{3}$$

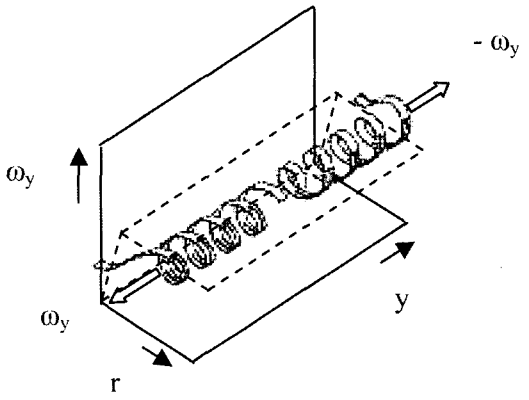

Figure 16. Representation of the stretched vortex filament and the streamlines induced around it.

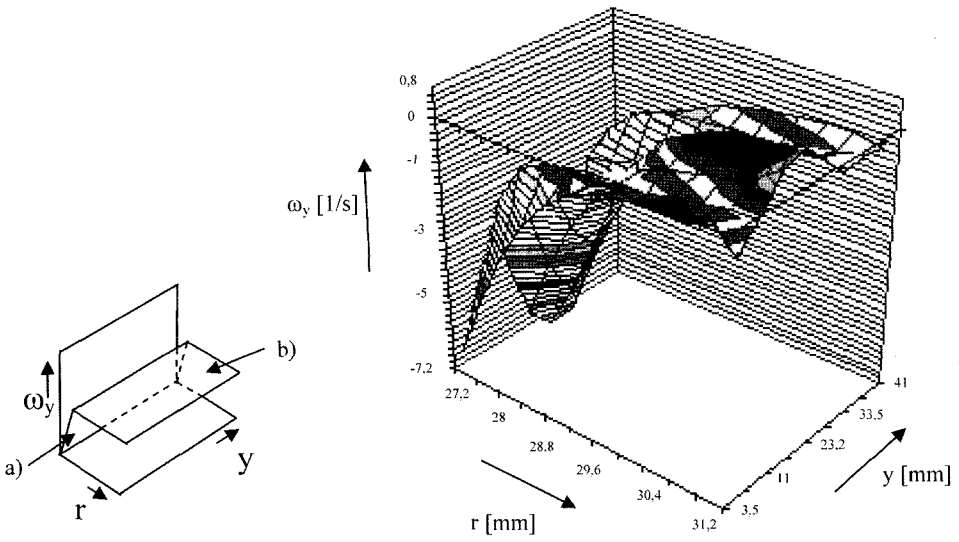

Figure 15. Fluid rotational at the inlet, upper cylinder 45 degrees, experimental.

Assuming the value of ω_y is constant as established in the previous section, the circulation associated to every "y" position will entirely depend on the vortex changing area. From the 3-D simulation in Figures 6 and 7, it can be seen that as the vortex reaches the cylinder edges, the vortex area diminishes. In reality, it also drops the velocity spiral and as a result, circulation will quickly decrease as the vortex breaks down. This phenomena was also corroborated during testing.

Conclusions

This paper defines and analyzes the main cause that prevents a further increase in production speed in pneumatic spinning processes.

It is demonstrated that as production speed increases, air currents generated by the pressing cylinders force the incoming fibres to change their previous direction turning them 90 degrees and therefore forcing the fibres to move along the pressing cylinders axis. As a result, fibres are not properly trapped by the cylinders and this leads to the creation of neps and other irregularities when forming the yarn.

These air currents have been studied experimentally, measured using a laser Doppler anemometer and also found via a 3D-CFD. In both cases, vorticity created at the cylinders inlet has been found.

The 3D- computer model has given a clear insight of vortex behaviour since it has shown the vortex dimensions and the vortex decay along the cylinders axis. Simulation has been very useful to discover the vortex distribution at the cylinders inlet when parameters such as the cylinders speed and dimensions are modified. CFD simulation has shown the complexity of the vortex created and also its breakdown effect in great detail.

Main vortex features have been studied theoretically revealing the vortex main line, direction and power associated.

Clear agreement between theory and simulation has been established, especially when regarding vortex position, vortex turning speed and vortex decay along the pressing cylinders axis.

Several methods to dispose of such undesirable vorticity have been studied, although just the use of drafting cylinders with holes and creating suction at its interior has given a good solution to the problem. As vortex creation is analyzed and understood, it opens a door to use the same solution in other applications.

Currently at INTEXTER-UPC, research is being carried out to develop optimum pressing cylinders. The aim is to direct the air currents appropriately and dispose of the associated vortex. As established in this paper, the use of a lower cylinder with holes will produce very interesting results in the near future.

Acknowledgements

We would like to express our most sincere gratefulness to Mr. J. Fresno, Mrs I. Gonzalez, Mrs. M. Domenech, Mr. F. Cano, Mr. A. Portero, Mr. J Fernandez, and Mr. L. Albañil, whose work has made this publication possible.

References

1. Batelle Institut, "Internal Report", 1981.
2. G. Konrad, *German Patent*, DE 03 511 (1976).
3. K. K. Murata Kikai, *German Patent*, DE 323799 (1982).
4. T. Jidoshokki, *GB Patent*, GB 2 115 019 A (1983), Japan Priority 57/007369 (1982).
5. Toray Industries Inc., *German Patent*, DE 24 16 880 (1974), Japan Priority JP 39991-73 (1973).
6. Y. Akira, *International Textile Bulletin*, **4**, 40 (2003).
7. K. Deno, *U. S. Patent*, 5.528.895 (1996).
8. L. Coll-Tortosa and T. T. Phoa, *Revista de la Industria Textil*, **150**, 88 (1977).
9. H. Stalder and J. Fischer, *ITS Textile Leader*, **15**, 51 (1994).
10. M. B. Hassen, F. Sakli, A. Sinoimeri, and M. Renner, *Text. Res. J.*, **73**(1), 55 (2003).
11. P. N. Duru and O. Babaarslan, *Text. Res. J.*, **73**(10), 907 (2003).
12. J. Lünenschloss, L. Coll-Tortosa, and T. T. Phoa, *Chemiefaser/Textil-Industrie*, **24/76**, 917, 1013 (1974).
13. J. Lünenschloss, L. Coll-Tortosa, and T. T. Phoa, *Chemiefaser/Textil-Industrie*, **24/76**, 355, 478 (1974).
14. P. Artzt and J. Bolze, *International Textile Bulletin*, **1**, 39 (1998).
15. K. P. S. Cheng and C. Yu, *Text. Res. J.*, **73**(4), 345 (2003).
16. R. A. Taylor and J. S. Graham, *Text. Res. Ins.*, **49**(12), 717 (1979).
17. P. Artzt, *International Textile Bulletin*, **5**, 26 (1998).
18. J. A. Tornero, J. M. Bergadà, F. Roig, E. Valencia, J. C. Sanchez, and Ll. Coll, "Flow Understanding and Visualization on a Pneumatic Spin Nozzle to Produce Yarn", 9th International Symposium on Flow Visualization, Edinburgh UK, August, 2000.
19. L. Prandtl, "The Generation of Vortices in Fluids of Small Viscosity", Wilbur Wright Memorial Lecture, Roy. Aer. Soc., **31**, 720 (1927).
20. H. Prümper, *Zeitschrift für Flugwissenchaften*, **20**(1/2), 60 (1972).
21. G. K. Batchelor, "Introduction to Fluid Dynamics", Cambridge University Press, 1967.